Phonon properties of GaAs/AlAs superlattice grown along the [110] direction

Z. V. Popović* and M. Cardona
Max-Planck-Institut für Festkörperforschung, Heisenbergstrasse 1, Postfach 80 06 65, D-7000 Stuttgart 80, Federal Republic of Germany

E. Richter and D. Strauch
Institut für Theorestische Physik, Universität Regensburg, D-8400 Regensburg, Federal Republic of Germany

L. Tapfer and K. Ploog
Max-Planck-Institut für Festkörperforschung, Heisenbergstrasse 1, Postfach 80 06 65, D-7000 Stuttgart 80, Federal Republic of Germany

(Received 20 April 1989)

We report Raman scattering studies of GaAs/AlAs superlattices grown along the [110] direction. The appearance of distinct x-ray satellite peaks around the Bragg reflections demonstrates the formation of highly ordered periodic superlattice structures. The confined-optical-phonon modes corresponding to the three optical bulk branches as well as the folded-acoustic-phonon modes are observed. The confined modes have frequencies which map closely onto those of the optical phonons of the parent materials in the [110] direction ($\Gamma-K-X$) of $\mathbf{k}$ space. We also observe resonant Raman scattering by confined-optical and in-plane (interfacelike) vibrational overtones and their combinations. The results of a lattice-dynamical calculation for this superlattice is also presented with special emphasis on angular dispersion and the mixed polarization of superlattice modes.

I. INTRODUCTION

In the last ten years, semiconductor superlattices have been the object of both theoretical and experimental investigation. Most of these studies have been performed on GaAs/AlAs superlattices grown on (001)-oriented GaAs substrates because of the smooth morphology of the epitaxial surface obtained for a large range of growth parameters and the excellent device behavior found with that orientation. More recently, it has been reported that high-quality heterostructures and superlattices can be grown by molecular-beam epitaxy (MBE) practically on any low-index crystallographic plane: (110),[1,2] (012),[3] (111),[4,5] (310),[5] (311),[6] and (211).[7] This opens the possibility to study many interesting phenomena which are strongly orientation dependent in quantum-well heterostructures and superlattices. The (110) GaAs layers and heterostructures are especially interesting because they may find important applications in electronics (e.g., avalanche devices and optical modulators for integrated optics).[1] In addition, it is known[8] that there are no intrinsic surface states in the fundamental band gap of an ideal reconstructed (110) surface of GaAs. This cleavage face is one of the preferred orientations for the growth of polar-nonpolar [e.g., zinc-blende (GaAs)–diamond (Si)] systems because the interface charge-imbalance problem can be avoided.[9] Until the work of Allen *et al.*[1] there was no report on the successful growth of device-quality heterostructures of (110) orientation.[6,8–10] Device-quality (110) GaAs has been reproducibly grown by MBE by tilting the GaAs substrate by 6° towards the (11$\bar{1}$) Ga-rich plane.[1] The growth of (110) GaAs/AlAs superlattices has been recently reported.[2] They were characterized using only nonpolarized Raman spectroscopy. From the lowered intensity of light scattering by folded phonons and much stronger intensity of resonance Raman scattering by interface modes, it was concluded that the (110) superlattices were of lower quality than the corresponding (001) GaAs/AlAs superlattices.

In this paper we present the results of x-ray and Raman scattering studies of a GaAs/AlAs superlattice grown along the [110] direction. The appearance of distinct satellite peaks around the Bragg reflections demonstrates the formation of a highly ordered periodic superlattice structure. The confined-optical-phonon modes corresponding to the three optical-bulk-phonon dispersion branches as well as folded LA-phonon modes are observed. The confined modes have frequencies which can be mapped closely onto the dispersion relations of the optical phonons of the parent materials. A calculation of the lattice dynamics of this superlattice is also given, where the mixed longitudinal and transverse character of the eigenmodes as well as the angular dispersion is investigated.

The remainder of this paper is organized as follows. After a brief description of the growth procedure and x-ray characterization (Sec. II), we consider symmetry and selection rules of Raman scattering of the (110) GaAs/AlAs superlattice (Sec. III). Experimental results are presented and discussed in Sec. IV. In Sec. V, the theoretical results for the superlattice modes are reported and compared with the experimental data. Section VI is used for a brief summary and conclusions.

II. EXPERIMENT

The GaAs/AlAs superlattices studied here were grown on (110) and, as a reference, simultaneously on (001) surfaces of GaAs by MBE in a three-chamber MBE system.

The (110) substrate was misoriented by 4.5° toward the (1$\bar{1}$3) plane to encourage the two-dimensional layer-by-layer growth mode and, thus, the formation of atomically smooth interfaces. Details of the preparation of the substrate surface prior to growth and of the conventional growth conditions are similar to those described elsewhere.[11] The growth rate of 0.5 monolayer/s for both GaAs and AlAs, as well as the shutter operation, were calibrated by monitoring the intensity oscillations of the reflection high-energy electron diffraction (RHEED) pattern on the (001) growth face. The growth temperature was kept below 550 °C to prevent diffusion across the interfaces.

The actual period of the superlattice was measured with a computer-controlled high-resolution double-crystal x-ray diffractometer. Figure 1 shows the experimental x-ray diffraction pattern of a (110) GaAs/AlAs superlattice recorded in the vicinity of the (220) GaAs reflection (Cu$K\alpha_1$ radiation). The measurement geometry is displayed on the inset of Fig. 1. This diffraction pattern was recorded with the geometry $|\gamma_n| < \gamma_0$,[12] where $\gamma_n = \cos[\pi/2-(\theta_B+\beta)]$ and $\gamma_0 = \cos[\pi/2-(\theta_B-\beta)]$ are the direction cosines of the diffracted beam, θ_B is the kinematical (220) Bragg angle, and β the angle between the (100) and (110) planes. The 0th-order superlattice peak (labeled by 0) is clearly separated from the GaAs substrate peak S, and the angular distance between these peaks is related to the ratio between the GaAs and AlAs layer thicknesses. The first-order satellite peaks $(+1,-1)$ are well pronounced and demonstrate the highly ordered periodic structure of the superlattice. The angular separation between the satellite peaks gives the superlattice period length. The values of superlattice parameters were obtained by simulation of the experimental diffraction curve using dynamical diffraction theory.[12] The thickness of the individual GaAs and AlAs layers were determined to be 26.0 and 27.5 Å, respectively. The interface roughness was found to be about two monolayers, which is twice that for superlattices grown along the [001] (Ref. 12) or [012] (Ref. 3) direction, and explains the increased full width at half maximum (FWHM) of the first-order satellite peaks. The Ga(Al)As layers are extremely thin, because both the Ga(Al) and As atoms are located on the same plane. The thickness of one (110) monolayer is about 2 Å (Fig. 2); thus the number of monolayers for the superlattice studied is 13 and 14 for GaAs and AlAs layers, respectively.

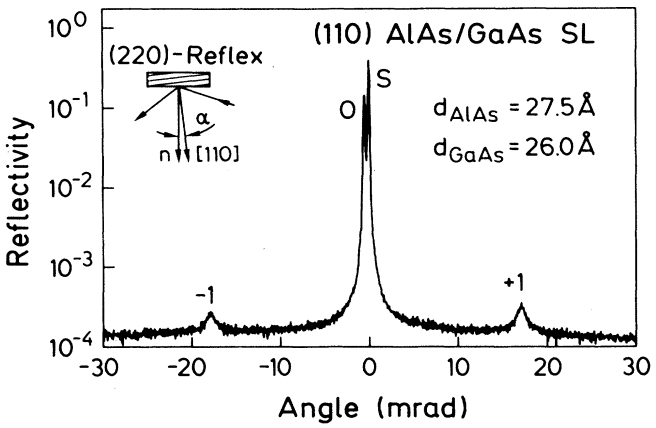

FIG. 1. Experimental double-crystal x-ray diffraction pattern of a (110) GaAs/AlAs superlattice recorded in the vicinity of the (220) GaAs reflection with Cu $K\alpha_1$ radiation. The zero on the angular scale refers to the (220) GaAs substrate peak (labeled S). The zeroth order (0) and first-order (± 1) satellite peaks are related to the superlattice. The angle between the surface normal n and the [110] direction is $\alpha = 4.5°$ towards the [1$\bar{1}$3] direction.

The Raman spectra were measured in the backscattering geometry using a conventional photon-counting detection system. The excitation light sources were the 5145-, 4880-, and 4579-Å lines of an Ar^+-ion laser and the 6471-Å line of a Kr^+-ion laser. Measurements were made both at room and liquid-nitrogen temperature.

III. SYMMETRY AND SELECTION RULES

It is well known[13] that in GaAs/AlAs superlattices superperiodicity in [001] direction induces a lowering of the crystal symmetry from cubic to tetragonal (point group D_{2d}). For the superperiodicity in the [110] direction the symmetry is orthorhombic (point group C_{2v}). The space-group analysis of $(GaAs)_{n_1}(AlAs)_{n_2}$ superlattices grown along the [110] direction is given in Table I and, depending on n_1 and n_2, results in four different space groups. The case $n_1 = n_2 = 1$ is equivalent to a (001) GaAs/AlAs superlattice.

Figure 2 shows a projection of the Ga(Al)As layers on the (1$\bar{1}$0) plane. In the same figure the symmetry operations of the C_{2v} point group are also indicated. The twofold axes (C_2) are parallel to [001], the z axis of constituents. The σ_v and σ_v' mirror planes are parallel to (110) and (1$\bar{1}$0), respectively.

In the ZnS structure the phonons propagating in the [110] direction have either pure transverse (y', parallel to [1$\bar{1}$0]) or mixed longitudinal (x') and transverse (z) polarization. The same is true for the modes with $\mathbf{q} \| [110]$ in (110) superlattices. With respect to the C_{2v} symmetry group the pure transverse (y') modes have either A_2 or B_2 symmetry; the mixed longitudinal and transverse ($x';z$) mode have A_1 or B_1 symmetry.

The Raman tensors for the optical modes (at bulk wave vector $\mathbf{k}=0$) of the ZnS structure of the parent crystals in the (x,y,z) coordinate system are

$$R(z) = \begin{bmatrix} 0 & d & 0 \\ d & 0 & 0 \\ 0 & 0 & 0 \end{bmatrix}_{k=0},$$

$$R(y') = \frac{1}{\sqrt{2}} \begin{bmatrix} 0 & 0 & -d \\ 0 & 0 & d \\ -d & d & 0 \end{bmatrix}_{k=0}, \quad (1)$$

$$R(x') = \frac{1}{\sqrt{2}} \begin{bmatrix} 0 & 0 & d \\ 0 & 0 & d \\ d & d & 0 \end{bmatrix}_{k=0},$$

where $R(x')$ corresponds to the LO modes at $\mathbf{k}=0$.

Besides the Raman tensors given by Eq. (1), we must also include the tensor

TABLE I. Symmetry of $(GaAs)_{n_1}$ $(AlAs)_{n_2}$ superlattices grown along the [110] direction.

Number of monolayers			Space
n_1	n_2	n_1+n_2	group
1	1	even	$P\bar{4}m2$ (D_{2d}^5)
even	even	even	$Pmn2_1$ (C_{2v}^7)
odd[a]	odd[a]	even	$Pmm2$ (C_{2v}^1)
even (odd)	odd (even)	odd	$Imm2$ (C_{2v}^{20})

[a]Except for $n_1=n_2=1$.

$$R_F=\begin{bmatrix} a & 0 & 0 \\ 0 & a & 0 \\ 0 & 0 & a \end{bmatrix}, \tag{2}$$

which results from the "dipole-forbidden" Fröhlich interaction of phonons of A_1 symmetry with nonvanishing longitudinal polarization.

The Raman selection rules for backscattering off the (110) surface of the parent material are given in Table II. In the following, we will assume that the same selection rules can be applied to the (110) GaAs/AlAs superlattices. In this case we only have to formulate the rules given in Table II with special emphasis on the confinement of the superlattice modes.

As in the (001) superlattices[14] one can assign effective wave vectors

$$q_m=m\frac{\pi}{d_i} \tag{3}$$

to modes confined to the constituents with effective layer thickness d_i (see Sec. V). Assigning these wave vectors, one takes into account the sinusoidal dependence of the envelope of confined-mode eigenvectors as a function of atomic-layer positions.

To the Raman-active confined pure transverse B_2 modes can be assigned effective wave vectors q_m with odd values of m; within the approximation for the Raman tensor, they should show up only in the depolarized spectrum (see Table II). The A_2 modes (with m even) are inactive. For illustration, an odd value of m leads to an even envelope function $[\cos(q_m x')]$ with respect to the center of the layer; see also Fig. 7. Incidentally, the B_2 representation of the corresponding eigenvector is the product representation of A_1, the representation of the envelope function, and B_2, the representation of the transverse displacements, while for the A_2 mode the envelope function has B_1 symmetry.

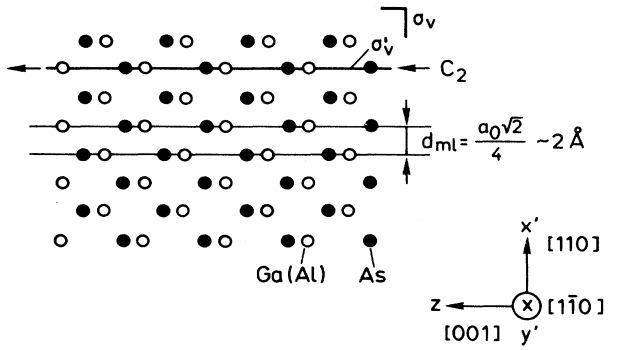

FIG. 2. (110) GaAs (AlAs) layers viewed along the [1$\bar{1}$0] direction. The symmetry elements of the C_{2v} point group are indicated.

For the mixed longitudinal and transverse A_1 modes (as far as they are accessible to our experiments) the longitudinal eigenvector component has an even value of m [$\sin(q_m x')$ envelope]; the envelope of the corresponding transverse component must have an odd m, which will thus be labeled $(m+1)$. The B_1 modes (with odd m) are inactive. For details see Sec. V, particularly for the determination of d_i and, hence, q_m. Let it suffice here to say that the calculated superlattice modes can be mapped well to the bulk dispersion branches using the effective wave vectors q_m as determined in Sec. V.

To simplify the phrasing concerning the mixed longitudinal and transverse confined modes in the following, we will label the modes mapping to the $\omega_1(k)$ bulk branch (Fig. 4) by LO_m with respect to their mainly longitudinal polarized eigenvectors for small values of q_m. Analogously, the modes mapping to the $\omega_3(k)$ bulk branch are labeled $TO_{z,m+1}$. In the case of the pure transverse modes, mapping to $\omega_2(k)$, we use $TO_{\perp z,m}$ in the text.

In order to determine the Raman selection rules for the folded acoustic phonons of the (110) superlattices, we also start from the selection rules and Brillouin tensors of the bulk crystals. For small bulk wave vector $\mathbf{k}$ along the [110] direction, i.e., in the linear dispersion region, besides the pure transverse $TA_{\perp z}$ (polarized along [1$\bar{1}$0]) modes there are nearly pure transverse (TA_z) phonons, polarized along the [001] axis and nearly longitudinal (LA) phonons. For larger $|\mathbf{k}|$, the phonons of the latter two branches have mixed longitudinal and transverse character.

The corresponding Brillouin tensors for TA and LA components are[15]

TABLE II. The polarization selection rules in the backscattering geometry for optical and acoustic phonons of GaAs/AlAs superlattices grown along the [110] direction as carried over from these for the bulk materials; a represents interband Fröhlich, d the deformation potential terms, and p_{ij} are elasto-optic constants.

			Light-scattering cross section				
	Incident	Scattering	Optical phonons			Acoustic phonons	
Configuration	polarization	polarization	A_1	B_2	TA_z	LA	$TA_{\perp z}$
$\bar{x}'(zz)x'$	[001]	[001]	a^2	0	0	$(\varepsilon_0^2 p_{12})^2$	0
$\bar{x}'(zy')x'$	[001]	[1$\bar{1}$0]	0	$d^2(TO_{\perp z})$	0	0	0
$\bar{x}'(y'y')x'$	[1$\bar{1}$0]	[1$\bar{1}$0]	$a^2+d^2(TO_z)$	0	0	$[(\varepsilon_0^2/2)(p_{11}+p_{12}-2p_{44})]^2$	0

$$R(\mathrm{TA}_z)=\frac{\varepsilon_0^2}{\sqrt{2}}\begin{vmatrix}0&0&p_{44}\\0&0&p_{44}\\p_{44}&p_{44}&0\end{vmatrix}_{k=0},$$

$$R(\mathrm{TA}_{\perp z})=\frac{\varepsilon_0^2}{2}\begin{vmatrix}p_{11}-p_{12}&0&0\\0&p_{12}-p_{11}&0\\0&0&0\end{vmatrix}_{k=0}, \quad (4)$$

$$R(\mathrm{LA})=\frac{\varepsilon_0^2}{2}\begin{vmatrix}p_{11}+p_{12}&2p_{44}&0\\2p_{44}&p_{11}+p_{12}&0\\0&0&2p_{12}\end{vmatrix}_{k=0},$$

where p_{ij} are the elasto-optic coefficients. Using these tensors, we have determined the selection rules for acoustic folded phonons as given in Table II. For (110) GaAs/AlAs superlattices within this approximation only the folded modes containing a longitudinal eigenvector component (i.e., A_1- and B_1-symmetry modes) should be Raman-active in backscattering. This is also the case for (001) GaAs/AlAs superlattices.[13]

IV. RAMAN SCATTERING SPECTRA

A. Confined phonons

Figure 3 shows the Raman spectra of the (110) $(\mathrm{GaAs})_{13}/(\mathrm{AlAs})_{14}$ sample for all three polarizations obtained at 80 K with the 5145-Å line, away from all resonances. For backscattering with both polarizations along the y' direction, phonons with both TO_z and LO eigenvector components are allowed (Table II). For the superlattice in the GaAs optical-phonon region, modes labeled LO_2 (291.8 cm^{-1}), LO_4 (281.7 cm^{-1}), LO_6 (274.7 cm^{-1}), $\mathrm{TO}_{z1}/\mathrm{TO}_{z3}$ (270.7 cm^{-1}), TO_{z5} (263.9 cm^{-1}), and TO_{z7} (257.3 cm^{-1}) are clearly observed [Fig. 3(a)]. The labeling implies the assigned dominant character of the eigenvectors as mentioned above, which will be discussed in more detail in Sec. V. The appearance of the LO_m (m even) and $\mathrm{TO}_{z,m}$ (m odd) confined modes for the $(y'y')$ configuration is in agreement with the selection rules and mixing scheme discussed above. In the AlAs optical-phonon region two confined modes at 362 cm^{-1} (TO_{z1}) and 400 cm^{-1} (LO_2) are observed. The additional broad peak at 390 cm^{-1}, labeled IF, is attributed by analogy with Refs. 16 and 17 to in-plane (interface) modes.

For the depolarized configuration [Fig. 3(b)] we observe, as expected from the selection rules of Table II, only $\mathrm{TO}_{\perp z,m}$ (m odd) confined modes. In the GaAs optical-phonon region three confined $\mathrm{TO}_{\perp z,m}$ modes at 271, 268.2 and 265.5 cm^{-1} ($m=1,3,5$) are clearly seen. In the AlAs region only one confined mode at 364 cm^{-1} ($\mathrm{TO}_{\perp z,1}$) is resolved.

For backscattering with both polarizations along z we expect to see only longitudinal confined modes LO_m and, because of their small longitudinal eigenvector component, a corresponding small contribution $\mathrm{TO}_{z,m+1}$ modes, in both cases with even m, i.e., spectra similar to those for backscattering with polarizations along y' with different relative weights. Actually, only one mode appears at the same frequency (281.7 cm^{-1}) for $(y'y')$ and (zz) polarization. This mode is positioned near the calculated values of the LO_4 (279.7 cm^{-1}) and also in-plane (interfacelike) mode frequencies at 281.7 281.4, and 280.2 cm^{-1} (see Sec. V). Its large intensity and width can be explained as a superposition of all these modes. The frequencies of other modes for the (zz) polarization differ from those for $(y'y')$ polarization. We believe that they originate, at least in part, from superlattice in-plane modes (these modes are equivalent to the "interface modes"[13]). We expect ir-active in-plane modes to separate from the confined ones since there is directional dispersion for $q\rightarrow 0$ (see Sec. V). The appearance of these modes for (zz) polarization requires some perturbation, yielding an in-plane wave-vector transfer, probably interface roughness.[16] This is the only possibility for appearance of other than LO_m confined modes with m even, because there are no polarization configurations in the (110) plane in which the LO modes of the parent crystals are Raman active. Further, it is known[17] that the diagonal Raman tensor components, allowed in principle for the superlattice (A_1 symmetry, point group C_{2v}) have very small values as calculated with the bond-polarizability model.[18,19] The clear appearance of LO_m (m even) modes for $(y'y')$ polarization [Fig. 3(a)] may come from the fact

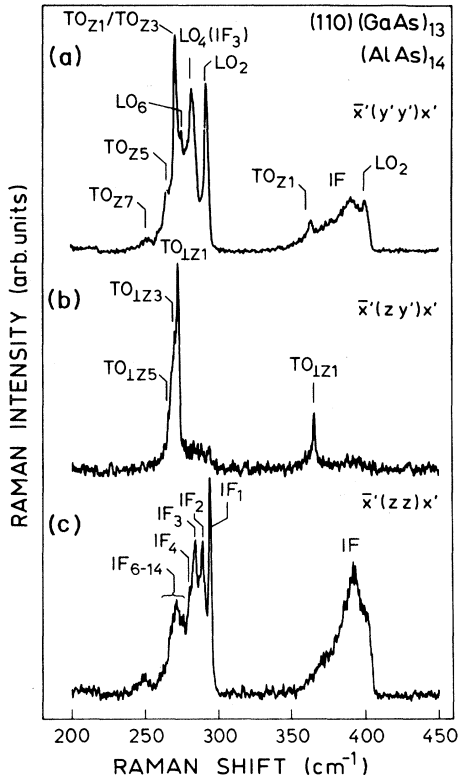

FIG. 3. Raman spectra of a $(\mathrm{GaAs})_{13}/(\mathrm{AlAs})_{14}$ superlattice at 80 K in (a) $\bar{x}'(y'y')x'$, (b) $\bar{x}'(zy')x'$, and (c) $\bar{x}'(zz)x'$ backscattering configurations ($\hat{\mathbf{x}}'\|[110]$, $\hat{y}'\|[1\bar{1}0]$, $\hat{\mathbf{z}}\|[001]$). The exciting laser line (5145 Å) is away from all resonances.

that with increasing m these modes have an increasing transverse eigenvector component and the scattering of light is "allowed" for this polarization (Table II). For (zz) polarization, Raman scattering by "transverse" modes is not allowed, and the in-plane modes may become dominant. Moreover, the frequency difference between the LO_2 confined mode for $(y'y')$ polarization and the corresponding mode (IF_1) for (zz) polarization is only 0.5 cm^{-1}. The calculated frequency difference between LO_1 and LO_2 modes (Sec. V) is 2.5 cm^{-1}, which means that the observed modes for (zz) polarization are not LO_m (m odd) modes for $\mathbf{q}\|[110]$, but, more likely, in-plane superlattice modes. The in-plane superlattice modes for $\omega > 279$ cm^{-1} (and small wave vector) have predominantly longitudinal character and their eigenvectors are a superposition of interface-type confined-mode eigenvectors with different q_m (with m odd, B_1 symmetry; see Fig. 7 for $\mathbf{q}\|[001]$). There are also small $TO_{z,m+1}$ components (B_1 symmetry), as suggested by Fig. 3(c). For details see Sec. V.

Using the assignment of observed Raman peaks to confined LO and TO modes as discussed above, we compare the corresponding frequencies with the dispersion relations of bulk GaAs and AlAs. This relations for wave vectors along the $\Gamma-K-X$ direction have been calculated using the shell model C (ii) of Dolling and Waugh[20] with parameters which give the best fit to recent low-temperature high-precision neutron data for GaAs.[21] The corresponding dispersion curves for AlAs were described by the same model with only the mass of the cation being changed. Figures 4(a) and 4(b) show the measured frequencies of LO_m, $TO_{\perp z,m}$, and $TO_{z,m}$ phonons versus q_m [for the definition of q_m, see Eq. (6) in Sec. V] together with the calculated dispersion curves of bulk GaAs and AlAs. In the same figure, the plotted bars represent the magnitude of the components of

$$\mathbf{e}_{ja}(\mathbf{q})/\sqrt{m_a} - \mathbf{e}_{jc}(\mathbf{q})/\sqrt{m_c} \tag{5}$$

along the three directions [110], [1$\bar{1}$0], [001]. Here $\mathbf{e}_{ja,c}(\mathbf{q})$ and $m_{a,c}$ are eigenvectors and masses of the anion (a) and cation (c), respectively. This representation helps in the identification of the dominant character of the vibrations and clearly exemplifies the LO-TO_z mixed-character bulk modes for $k \neq 0$ as much as the pure transverse character of the $TO_{\perp z}$ modes.

As seen in Fig. 4(a), the agreement between our experimental data for GaAs optical phonons and the theoretical predictions is rather good, especially for the pure transverse $TO_{\perp z,m}$ confined phonons. In the AlAs optical-phonon region, we observed only one confined-phonon mode for each optical branch. The difference between experimental and theoretical frequencies is less than 3 cm^{-1} [typical also of (001) GaAs/AlAs superlattices[22]]. We believe that this difference originates from insufficient accuracy of the calculated dispersion curves

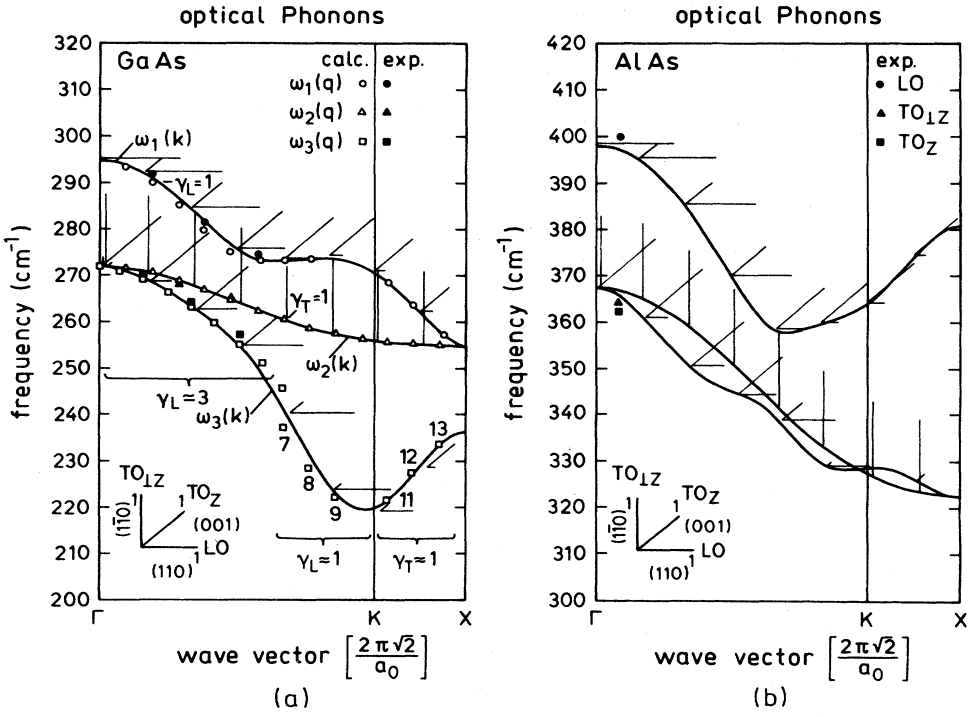

FIG. 4. Experimental (●,▲,■) and calculated (○,△,□) confined-mode frequencies as a function of confinement wave vector $q_m = [m/(n_i + \gamma_{L,T})](2\pi\sqrt{2}/a_0)$, see Eq. (6), together with theoretical optical-phonon dispersion curves of (a) bulk GaAs and (b) AlAs in the $\Gamma-K-X$ direction and the projections of the corresponding phonon displacements of the cation relative to the nearest anion [Eq. (5)] along the [110], [1$\bar{1}$0], and [001] directions.

of bulk AlAs, for which no neutron scattering data are available.

B. Resonant scattering

Figure 5 shows Raman spectra of the (110) $(GaAs)_{13}/(AlAs)_{14}$ sample obtained at 80 K with the 6471-Å line of a Kr^+-ion laser. This photon energy is near resonance with the first heavy-hole–electron exciton transition of these GaAs quantum wells. Six strong bands arise between 500 and 1100 cm^{-1}. We identify them as overtones of GaAs confined phonons (modes between 550 and 600 cm^{-1} and between 850 and 900 cm^{-1}) and of the AlAs interface mode (mode at 778 cm^{-1}) and as a combination of the two (modes between 650 and 700 cm^{-1} and between 900 and 1100 cm^{-1}). These modes, as well as the AlAs first-order optical modes, are seen for all three polarizations. The observed first-order spectra of the optical phonons of GaAs are the same for both polarized configurations, as shown in the inset of Fig. 5, contrary to the results obtained out of resonance (Fig. 3). The appearance of different first-order spectra in resonance for polarized and depolarized configurations is not surprising for the (110) superlattice. The reason is that in the depolarized configuration, according to Table II, only

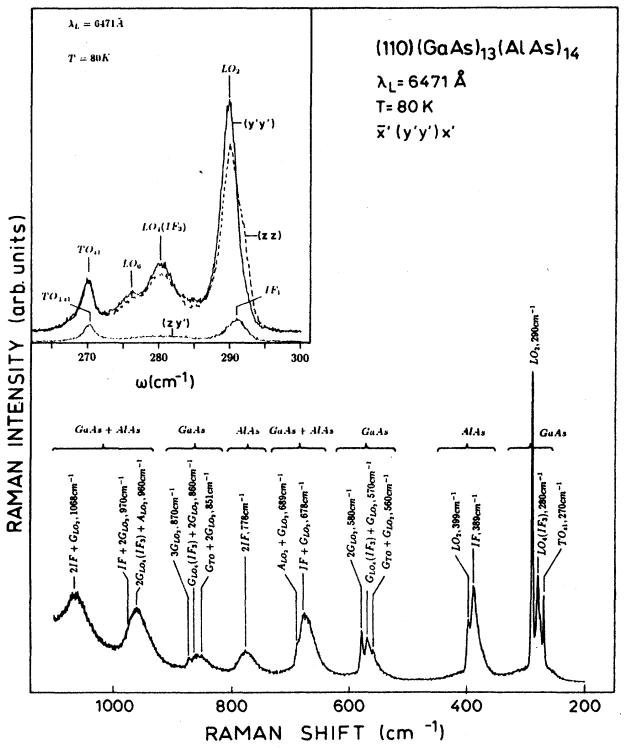

FIG. 5. Raman spectra of a $(GaAs)_{13}/(AlAs)_{14}$ superlattice at 80 K in the $\bar{x}'(y'y')x'$ configuration. The exciting laser line $\lambda_L = 6471$ Å is very close to resonance conditions. Inset: first-order Raman spectra in the GaAs optical-phonon region for all three polarizations.

confined modes of the purely transverse TO_{1z} branch are allowed. For higher-order scattering we find, as mentioned above, the same spectra for all principal polarizations. The mode near 292 cm^{-1} with predominantly longitudinal character seen in the (zy') configuration (inset in Fig. 5) is probably an in-plane mode induced by leakage or defects, as discussed above. All modes observed in resonance for a polarized configuration are either confined modes of A_1 symmetry or in-plane modes. Due to the absence of LO_m and $TO_{z,m}$ modes of B_1 symmetry in the first- and higher-order spectra, we conclude that the scattering by the modes observed in resonance is induced by Fröhlich interaction.[16,17]

C. Folded acoustic phonons

As mentioned above, the propagation properties of acoustic waves in a superlattice can be obtained from the propagation of acoustic waves in the parent materials. In anisotropic materials, three waves propagate for a given direction of **q**, but for a general **q** the displacements are not along or perpendicular to the direction of propagation, so that these waves are not strictly longitudinal or transverse. There are special directions, however, for which the particle motions are either along (pure longitudinal) or perpendicular (pure transverse) to the direction of propagation. For cubic solids (e.g., GaAs) there are three directions of propagation ($\langle 100\rangle$, $\langle 110\rangle$, and $\langle 111\rangle$) for which the long-wavelength acoustic waves have pure longitudinal and transverse character.[23] For the $\langle 100\rangle$ and $\langle 111\rangle$ directions of propagation the two transverse modes are degenerate. In the $\langle 110\rangle$ direction of propagation, transverse-acoustic waves are not degenerate, although they are pure transverse. (As mentioned above, this is only valid in the continuum approximation.) The velocities of these waves are[23]

$$v_{\text{long}} = [(c_{11}+c_{12}+2c_{44})/2\rho]^{1/2} \quad \text{along } [110] ,$$

$$v_{\text{trans}} = (c_{44}/\rho)^{1/2} \quad \text{along } [001] ,$$

$$v_{\text{trans}} = [(c_{11}-c_{12})/2\rho]^{1/2} \quad \text{along } [1\bar{1}0] ,$$

where c_{11}, c_{12}, and c_{44} are the stiffness constants and ρ is the mass density.

Raman scattering by folded acoustic phonons in (001)-oriented GaAs/AlAs superlattices is well documented.[13] Because of difficulties in preparing high-quality superlattices on other than (001)-oriented substrates, the observation of folded phonons propagating in other than the [001] direction was not possible until recently.[2,24]

As predicted by the selection rules of Table II, only folded-acoustic-phonon modes with longitudinal eigenvector components are Raman active for (110)-oriented superlattices. Figure 6 shows the Raman spectra for (zz) polarization in the spectral range between 20 and 50 cm^{-1} obtained at 300 K with the 4579-Å line of an Ar^+-ion laser. The doublet $(-1,+1)$ of folded-LA-phonon modes at 32 and 38.5 cm^{-1} is clearly observed. In addition to the LA doublet in Fig. 6, there are weaker features between 17 and 27 cm^{-1}. We assign a shoulder at about 19 cm^{-1} to the $+1$ component of the TA_{1z} dou-

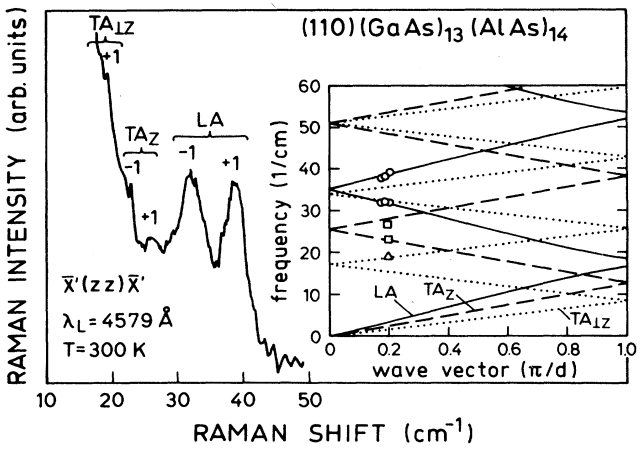

FIG. 6. Raman spectra of a $(GaAs)_{13}/(AlAs)_{14}$ superlattice in the spectral region from 20 to 50 cm^{-1} measured with the 4579-Å line of an Ar^+-ion laser at 300 K. The inset shows continuum-model results for folded-phonon dispersion curves together with experimentally observed LA (○), TA_z (□), and $TA_{\perp z}$ (△) folded phonons.

blet and the peaks at 23 and 26 cm^{-1} to the TA_z (± 1) doublet, since their position is in reasonable agreement with continuum-model calculations (inset of Fig. 6). These modes are actually forbidden by the selection rules of Table II, but may be induced by deviations from exact backscattering or by forward scattering resulting from reflection at the superlattice-substrate interface. Note that the TA_z mode may also be activated by a piezoelectric coupling.[25]

We have compared the frequencies of the observed folded-phonon modes with a calculation based on the continuum model. Folded-phonon dispersion curves calculated with this model are given in the inset of Fig. 6 together with the experimental frequencies obtained with the 4579-, 4880-, and 5145-Å lines of an Ar^+-ion laser. Our experimental data for LA folded phonons in the [110] direction are fully in agreement with the continuum-model calculation, which means that the stiffness constants taken for the bulk materials[26] are correct. (The calculation within the shell model leads to the same results.)

V. LATTICE DYNAMICS OF THE SUPERLATTICE

Lattice-dynamical calculations were performed for the (110) $(GaAs)_{13}/(AlAs)_{14}$ superlattice using the shell model *C*(ii) of Dolling and Waugh,[20] previously applied to (012) GaAs/AlAs superlattices.[3] A different model was used in the study of (001) superlattice, but, with readjusted parameter, the shell model was found[21] to give a better fit to the neutron data. In the following, we will consider only confined modes out of the GaAs optical-frequency region.

Figure 7 shows frequencies and relative-displacement vectors of an anion-cation pair for some of the confined modes of the (110) $(GaAs)_{13}/(AlAs)_{14}$ superlattice. The left panel of Fig. 7 shows the displacement vectors for a

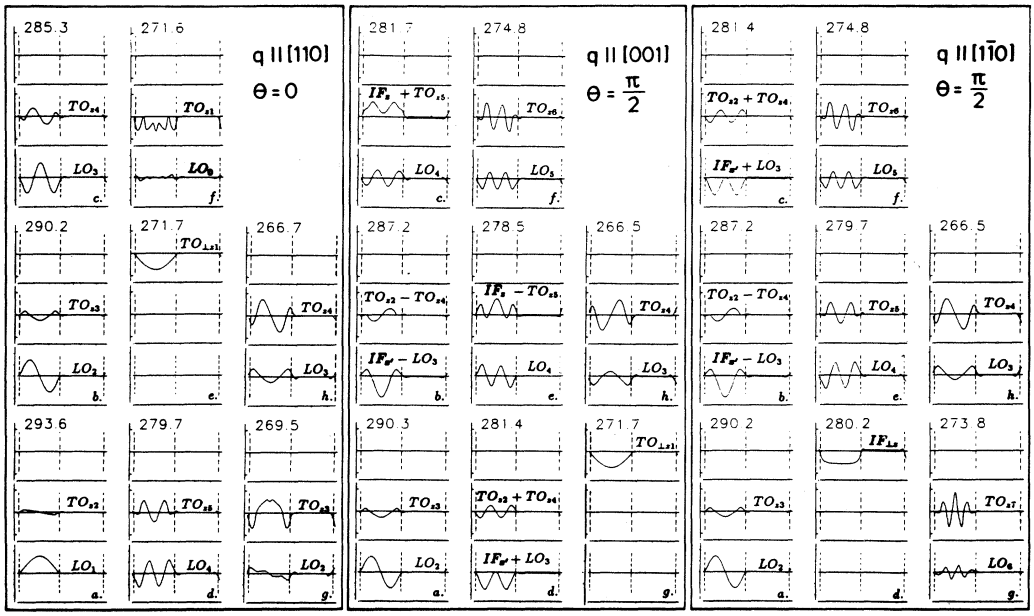

FIG. 7. Displacement vectors for a number of GaAs-like zone-center optical modes for a $(GaAs)_{13}/(AlAs)_{14}$ superlattice. Plotted are the optical relative-displacement vectors of anion-cation pairs along the layer axis [see Eq. (5); the anion and cation of one pair belong to the same plane perpendicular to the layer axis]. Left panel, **q** approaches zero along the [110] direction ($\theta=0$); middle and right panels, **q** approaches zero along the [001] and [1$\bar{1}$0] directions ($\theta=\pi/2$).

very small $\mathbf{q}$ along the growth direction ($\theta=0$), and the middle and right panels those for small in-plane $\mathbf{q}$ along [001] and [1$\bar{1}$0], respectively ($\theta=\pi/2$).

The confined modes with $\mathbf{q}\|[110]$ and $q\sim 0$ have eigenvectors whose sinusoidal dependence as a function of monolayer position can be described by effective wave vectors q_m,

$$q_m = m\frac{\pi}{d_i} \quad \text{with } d_i=(n_i+\gamma_{\mathrm{L,T}})\frac{a_0}{2\sqrt{2}} , \tag{6}$$

$a_0/2\sqrt{2}$ being the thickness of one monolayer and n_i the number of GaAs or AlAs monolayers, respectively. The values γ_{L} and γ_{T} describe the extent to which the modes confined to one (GaAs) layer penetrate into the other (AlAs).

For the confined pure transverse $\mathrm{TO}_{\perp z,m}$ modes, we find best agreement with the bulk modes for $\gamma_{\mathrm{T}}\approx 1$, a result familiar from the (001) GaAs/AlAs superlattices.[14] With this choice of d_i the frequencies of these modes map closely on the $\omega_2(k)$ bulk branch; see Fig. 4(a). As an example, the displacement vector components of the $\mathrm{TO}_{\perp z,1}$ mode are given in Fig. 7(e) (left panel).

For the confined superlattice modes with mixed longitudinal and transverse (LO-TO_z) polarization [corresponding to the $\omega_1(k)$ and $\omega_3(k)$ bulk branches] the eigenvector components can be described by effective wave vectors q_m, Eq. (6), to be detailed shortly. For a given m, the longitudinal component, labeled LO_m, has $m-1$ nodes (m extrema), while the transverse component has one additional node; hence it will be labeled $\mathrm{TO}_{z,m+1}$. The eigenvectors, particularly the transverse components, are small near and beyond the interface.

The determination of the effective wave vector for the confined LO-TO_z modes is far more complicated than in the pure TO case due to (partially) overlapping bands in the bulk crystal, cf. Fig. 4(a): the ω_1 and ω_3 branches have a common frequency region at about 255–270 cm^{-1}; two different sections of the ω_3 branch occur in the 220–235-cm^{-1} region, and the minimum of the ω_3 branch and the maximum of an acoustic branch [not shown in Fig. 4(a)] is found near 220 cm^{-1}. The following rules seem to emerge from the analysis of the LO-TO_z mode eigenvectors.

(i) The eigenvectors of the modes with frequencies from the ω_1 branch are well described with $\gamma_{\mathrm{L}}=1$. Displacement vector components for modes of this kind are shown in Figs. 7(a)–7(d) (left panel).

(ii) The LO_m modes with $m=9$ and 10 are missing; this occurs where the expected LO_9 and LO_{10} frequencies would reach the top of the ω_3 band (at 272 cm^{-1}), and mixing of the backfolded ω_1 and ω_3 modes is possible.

(iii) Instead of the two missing LO_m modes, two $\mathrm{TO}_{z,m+1}$ modes with $m=0$ and 1 occur (classified according to their longitudinal eigenvector component) with remarkable admixture of K-point character [see Figs. 7(f) and 7(g) in the left panel].

(iv) In the $\mathrm{TO}_{z,m}$ band, one finds three different regions of $\mathbf{q}=(\xi\xi 0)2\pi\sqrt{2}/a_0$ with different values for γ:

(a) In the 270–245-cm^{-1}, $0<\xi<\frac{1}{2}$ mixed LO-TO region one finds $\gamma_{\mathrm{L}}\sim 3$.

(b) For $\frac{1}{2}<\xi<\frac{3}{4}$ one finds $\gamma_{\mathrm{L}}\sim 1$. As far as the eigenvector is concerned, this branch section is the continuation of the $\omega_1(k)$ branch starting at 295 cm^{-1} with that same γ_{L}. This is called eigenvector exchange. These modes are labeled $m=7,8,9$.

(c) For $\frac{3}{4}<\xi\leq 1$ one has another eigenvector exchange with a predominantly transverse-acoustic branch section (not shown in Fig. 4), and in the obvious $\mathrm{TO}_{z,m}$ notation one finds $\gamma_{\mathrm{T}}\sim 1$ for the wave vector q_m with $m=11,12,13$. The mapping procedure leaves the $m=10$ position near the K point empty. This mode can be found as a slightly confined (to the GaAs layer) mode belonging to the TA_z branch (not indicated in Fig. 4).

(d) There are transition regions (for $\gamma_{\mathrm{L,T}}$) that have been neglected in the data shown in Fig. 4(a). The mismatch of mapping around the frequency of 245 cm^{-1} in Fig. 4(a) is thus due to the abrupt change of γ_{L} from 3 to 1 and of m from 9 to 7 in the calculation of the effective wave vector with Eq. (6).

We now refer to the middle and right panels of Fig. 7. As in the case of (001) (Ref. 27) and (012) (Ref. 3) superlattices the displacement vectors of some modes propagating parallel (left panel of Fig. 7) and perpendicular (middle and right panel) to [110] are quite different. Typically for heteropolar uniaxial crystals, the (110) superlattice modes show angular dispersion at the Γ point (unretarded calculation).

(1) The modes with ir activity (A_1, B_1, and B_2) exhibit angular dispersion for small values of $|\mathbf{q}|$, i.e., they are singular functions of $\mathbf{q}$ for $\mathbf{q}\rightarrow\mathbf{0}$. This dispersion is displayed in Figs. 8(a) and 8(b). For the ir dipole moment parallel to the wave vector $\mathbf{q}$ the modes are "LO-like" and thus have a higher frequency than for directions perpendicular to $\mathbf{q}$. In this case of an in-plane $\mathbf{q}$ the modes are superpositions of confined modes and the "interface modes" ($\mathrm{IF}_{x'}$, $\mathrm{IF}_{\perp z}$, and IF_z), as obtained in the electrostatic approximation.[28] For the IF modes, there is nonvanishing amplitude in both layers, and for $|\mathbf{q}|\neq 0$ the eigenvectors show exponential decay along x' within each layer. Since these kinds of interface modes in macroscopic, exponential decay are not obvious in our calculated eigenvectors ($|\mathbf{q}|\approx 0$), and with respect to the superposition, we prefer to use the term "in-plane modes." However, we emphasize the fact that interface modes are simply ir-active in-plane modes (regarding the superlattice as a uniaxial crystal). A large frequency shift exists between the corresponding ir-active modes propagating parallel and perpendicular to the layer axis. Generally this discontinuity is different for $\mathbf{q}$ approaching zero from different in-plane directions; see Figs. 8(a) and 8(b).

(2) $\mathrm{TO}_{\perp z,m}$ modes of m even (A_2-symmetry modes) have no angular dispersion; for m odd (B_2-symmetry modes) the dispersion is negligible for all m except $m=1$ [compare Fig. 7(e), left panel, and Fig. 7(d), right panel]. [Note that the B_2 mode of Fig. 7(d) is the only pure interface mode shown in Fig. 7.] Since B_2 modes have the ir dipole moment parallel to (1$\bar{1}$0), no dispersion occurs for $\mathbf{q}$ varying in the (110)-(001) plane.

(3) For in-plane wave vectors $\mathbf{q}$, A_1- and B_1- symmetry

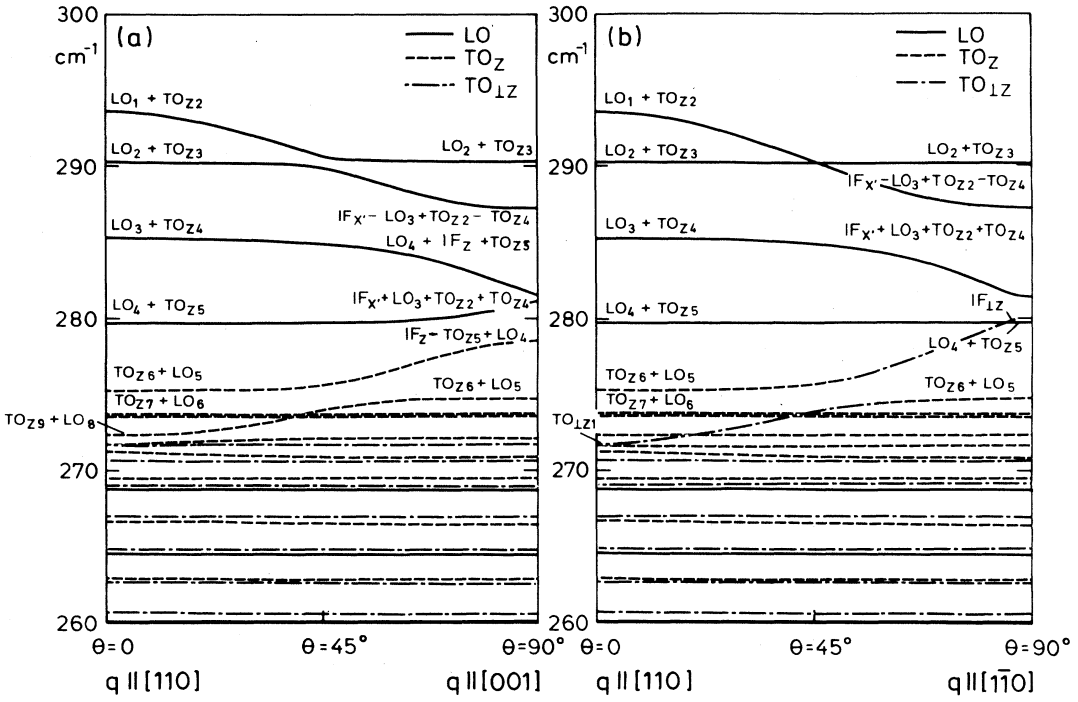

FIG. 8. Calculated angular dispersion of the optical modes of a $(GaAs)_{13}/(AlAs)_{14}$ superlattice for infinitesimal **q**. (a) **q** in the (x',z) plane; (b) **q** in the (x',y') plane. The solid lines represent modes predominantly polarized along x' (LO), while the dashed and the dashed-dotted lines correspond to predominant TO_z and $TO_{\perp z}$ polarizations.

modes have mixed interface–confined-mode character for frequencies above 270 cm^{-1} [see the anticrossing in Fig. 8(a); below 270 cm^{-1} angular dispersion is negligible]. Some modes of this kind are shown in (b), (c), and (d) of the middle panel of Fig. 7, and in (b), and (c) of the right panel.

(4) The influence of the macroscopic field disturbs the crystal symmetry (unretarded calculation). For **q** varying in the $(1\bar{1}0)$ plane [Fig. 8(a)] A_1 and B_1 belong, therefore, to the same symmetry class [odd with respect to $(1\bar{1}0)$ reflection]. Similarly A_2 and B_2 are both even. Thus, anticrossing can occur in the dispersion branches of A_1 and B_1 modes (the pure transverse A_2 and B_2 show no angular dispersion).

For **q** varying in the (001) plane [Fig. 8(b)], there exists only one irreducible representation. The reason for the apparent crossing of dispersion branches in Fig. 8(b) is that the ir dipole moment of these modes is parallel to the [001] direction, which makes them transverse for any direction of **q** in this plane.

In Figure 9 we compare the measured Raman spectra of the GaAs optical-phonon region of our superlattice with the theoretical results. The calculated frequencies of the confined-superlattice modes are represented by solid vertical lines and in-plane (interfacelike) modes with small $|\mathbf{q}|$ by dashed ($\mathbf{q}\|[100]$) or dotted ($\mathbf{q}\|[1\bar{1}0]$) lines. Satisfactory agreement between experimental assignments and calculated frequencies of confined phonons is found. Nevertheless, one has to keep in mind that the theoretical results for the eigenvectors (more than for frequencies) in the case of the confined LO-TO mixed modes may depend sensitively on the model used, due to the model-dependent anticrossing effects.

The calculations give confined-mode frequencies about 1 cm^{-1} lower than experimentally observed (for LO_m as well as for $TO_{z,m+1}$ modes), which is the same as the resolution and absolute accuracy in the frequencies of the Raman spectra. This comparison can also explain the large intensity and broadening of the "LO_4" peak as a superposition of the LO_4 confined mode with in-plane modes at about 281.7 cm^{-1} (propagating in the [100] direction), 280.2 cm^{-1} (propagating in the $[1\bar{1}0]$ direction), and 281.4 cm^{-1} (one propagating in the [100] and one in the $[1\bar{1}0]$ direction; see Fig. 8(b)). These in-plane modes are denoted in Fig. 9 as IF_3. The agreement is especially good for the $TO_{\perp z,m}$ confined modes.

For the (zz) polarization one should see, induced by the Fröhlich interaction, only LO_m, $TO_{z,m+1}$ (m even) modes, and interface modes. The peak observed at 292.3 cm^{-1} (IF_1) may correspond to LO_2, except that it is found at higher frequencies (~ 0.5 cm^{-1}) than the LO_2 peak seen in the $(y'y')$ configuration. Since the latter is allowed by its $TO_{z,2+1}$ admixture (Table II), we conclude that the "LO_2" (IF_1) peak in the (zz) configuration originates from a mode with a wave-vector direction different from [110] and frequency slightly higher due to the an-

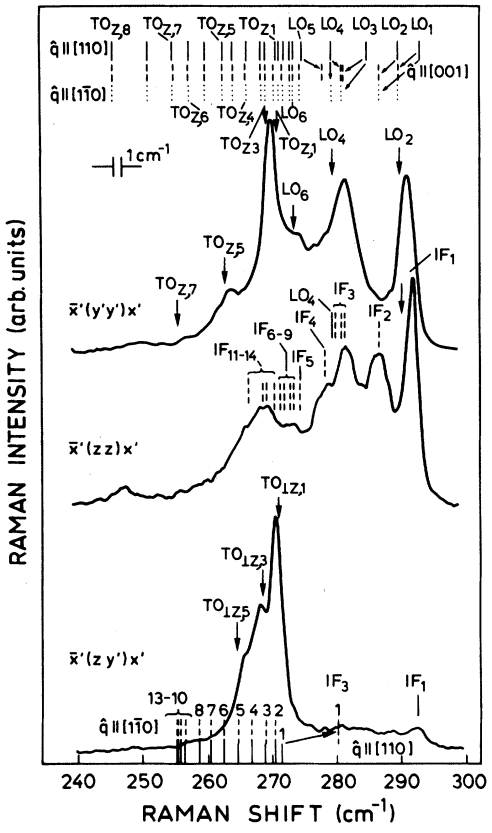

FIG. 9. Comparison of Raman spectra in the GaAs optical-phonon region with calculated frequencies for the $(GaAs)_{13}/(AlAs)_{14}$ superlattice. The position of calculated confined phonons is represented by vertical solid lines (for $\mathbf{q}\|[110]$, $\theta=0$) and dashed and dotted lines for in-plane (interfacelike) modes propagating along the [001] and [1$\bar{1}$0] directions, respectively ($\theta=\pi/2$).

ticrossing seen in Fig. 8(a). The peak at 287 cm^{-1} corresponds well to the IF_2 ($IF_{x'}$-LO_3) in-plane mode while the shoulder (IF_4) found at 278.5 cm^{-1} can be correlated with the IF_z-$TO_{z,5}$ interface mode, Fig. 8(a), found for $\mathbf{q}$ along [001]. The next two shoulders, at 273.5 and 269.2 cm^{-1}, are denoted as superpositions of several in-plane modes as indicated in Fig. 9.

VI. SUMMARY

We have investigated the phonon properties of a $(GaAs)_{13}/(AlAs)_{14}$ superlattice grown along the [110] direction. Good-quality superlattices of this orientation have been grown by MBE tilting the (110) GaAs substrate by 4.5° towards the (1$\bar{1}$3) plane. The appearance of distinct x-ray satellite peaks demonstrates the formation of highly ordered periodic superlattice structures. The interface roughness was found to encompass about two monolayers. We have observed confined-optical-phonon modes of all three phonon dispersion branches up to sixth order. These modes have frequencies which map closely onto those of the optical phonons of the parent materials in the $\Gamma-K-X$ direction ([110]) of $\mathbf{k}$ space. We have also observed resonant Raman scattering by confined-optical and interface-vibrational overtones and their combinations. Folded-acoustic-phonon doublets whose frequencies are in agreement with continuum-model calculations have also been seen.

We have performed a shell-model calculation of the phonon frequencies and eigenvectors of a (110) $(GaAs)_{13}/(AlAs)_{14}$ superlattice. The zone-center optical modes display angular anisotropy. The calculated normal-to and in-plane modes show good agreement with measured TO and LO confined- and interface-mode frequencies in the GaAs optical-phonon region. The assignment of effective wave vectors q_m to confined modes in the (110) superlattice has been found to be more complicated than in the (001) case. This complication can be traced back to the existence of several bulk branches or branch sections of the same frequency and symmetry, in our case the mixed longitudinal-transverse phonon branches near 270 and 220 cm^{-1}. Our investigations seem to indicate that the proper assignment of q_m can only be made by reference to theoretical eigenvector envelope functions: one has to keep in mind, however, that different models may give slightly different results.

ACKNOWLEDGMENTS

The technical assistance of A. Fischer with MBE growth and H. Hirt, M. Siemers, and P. Wurster with Raman measurements is gratefully acknowledged. Part of this work was sponsored by the Bundesministerium für Forschung und Technologie of the Federal Republic of Germany. One of us (Z.V.P) gratefully acknowledges financial support by the Alexander von Humboldt Foundation (Bonn, Germany).

*Permanent address: Institute of Physics, P.O. Box 57, YU-11000 Belgrade, Yugoslavia.

[1]L. T. P. Allen, E. R. Weber, J. Washburn, and Y. C. Pao, Appl. Phys. Lett. **51**, 670 (1987).

[2]D. Kirillov and Y. C. Pao, in *Epitaxy of Semiconductor Layer Structures,* Mater. Res. Soc. Symp. Proc. No. 102, edited by R. T. Tung, L. R. Dawson, and R. L. Gunshor (MRS, Pittsburgh, 1988), p. 169.

[3]Z. V. Popović, M. Cardona, E. Richter, D. Strauch, L. Tapfer, and K. Ploog, Phys. Rev. B **40**, 1207 (1989).

[4]T. Hayakawa, K. Takahashi, M. Kondo, T. Suyama, S. Yamamoto, and T. Hijikata, Phys. Rev. Lett. **60**, 349 (1988).

[5]L. W. Molekamp, G. E. W. Bauer, R. Eppenga, and C. T. Foxon, Phys. Rev. B **38**, 6147 (1988).

[6]T. Fukunaga, T. Takamori, and H. Nakashima, J. Cryst. Growth **81**, 85 (1987).

[7]S. Subbana, H. Kroemer, and J. L. Merz, J. Appl. Phys. **59**, 488 (1986).

[8]W. I. Wang, J. Vac. Sci. Technol. B **1**, 630 (1983).
[9]W. I. Wang, Surf. Sci. **174**, 31 (1986).
[10]P. M. Petroff, A. Y. Cho, R. K. Reinhart, A. C. Gossard, and W. Wiegmann, Phys. Rev. Lett. **48**, 170 (1982)
[11]T. Isu, D. S. Jiang, and K. Ploog, Appl. Phys. A **43**, 75 (1987).
[12]L. Tapfer and K. Ploog, Phys. Rev. B **33**, 5565 (1986); L. Tapfer, Phys. Scr. T **25**, 45 (1989).
[13]B. Jusserand and M. Cardona, in *Light Scattering of Solids V,* edited by M. Cardona and G. Güntherodt (Springer-Verlag, Heidelberg, 1989), p. 49.
[14]B. Jusserand and D. Paquet, Phys. Rev. Lett. **56**, 1752 (1986).
[15]H. Z. Cummins and P. E. Schoen, in *Laser Handbook,* edited by F. T. Arecchi and E. O. Schulz-Dubois (North-Holland, Amsterdam, 1972), p. 1029.
[16]A. K. Sood, J. Menéndez, M. Cardona, and K. Ploog, Phys. Rev. Lett. **54**, 2115 (1985).
[17]A. Alexandrou, M. Cardona, and K. Ploog, Phys. Rev. B **38**, 2198 (1988).
[18]A. K. Sood, J. Menéndez, M. Cardona, and K. Ploog, Phys. Rev. Lett **54**, 2111 (1985).
[19]A. S. Barker, Jr., J. L. Merz, and A. C. Gossard, Phys. Rev. B **17**, 3181 (1978).
[20]G. Dolling and J. L. T. Waugh, in *Lattice Dynamics,* edited by R. F. Wallis (Pergamon, Oxford, 1965), p. 19.
[21]D. Strauch and B. Dorner (unpublished).
[22]Z. P. Wang, D. S. Jiang, and K. Ploog, Solid State Commun. **65**, 661 (1988).
[23]B. A. Auld, *Acoustic Fields and Waves in Solids* (Wiley, New York, 1973), Vol. 1, 191; C. Kittel, *Introduction to Solid State Physics* (Wiley, New York, 1953), p. 121.
[24]Z. V. Popović, H. J. Trodahl, M. Cardona, E. Richter, D. Strauch, and K. Ploog, Phys. Rev. B **40**, 1202 (1989).
[25]G. Winterling, E. S. Koteles, and M. Cardona, Phys. Rev. Lett. **39**, 1286 (1977).
[26]*Landolt-Börnstein,* Vol. 17a: *Physics of Group IV Elements and III-V Compounds,* edited by O. Madelung (Springer, Berlin, 1982), p. 235. The following values of elastic constants for GaAs (AlAs) are used: $c_{11}=11.84\times10^{11}$ (12.5×10^{11}) dyn/cm^2, $c_{12}=5.37\times10^{11}$ (5.34×10^{11}) dyn/cm^2, and $c_{44}=5.91\times10^{11}$ (5.42×10^{11}) dyn/cm^2.
[27]E. Richter and D. Strauch, Solid State Commun. **64**, 867 (1987).
[28]R. E. Camley and D. L. Mills, Phys. Rev. B **29**, 1685 (1984).